25th ABCM International Congress of Mechanical Engineering
October 20-25, 2019, Uberlândia, MG, Brazil

COBEM2019-0804
STUDY OF AN ISOLATED GAS BUBBLE DYNAMICS IN A CENTRIFUGAL ROTOR

Higor Leandro Veiga da Silva
Edgar Ofuchi
Henrique Stel
Ernesto Mancilla
Dalton Bertoldi
Rigoberto E. M. Morales
Federal University of Technology – Paraná – UTFPR, Multiphase Flow Research Center – NUEM.
Rua Dep. Heitor Alencar Furtado 5000, Curitiba, 81280340, Brazil
higorveiga_@hotmail.com, edgarofuchi@gmail.com, stel.henrique@gmail.com, ernesto.mancilla@icat.unam.mx, daltonbertoldi@utfpr.edu.br, rmorales@utfpr.edu.br

Abstract. *Nowadays, electrical submersible pump (ESP) is one of the most common artificial lift technique in the petroleum industry. However, due to the presence of gas in most of oil reservoirs, the ESP may operate in two-phase flow conditions. In this case, the presence of gas in the rotor channels of the pump can cause a performance degradation, reducing its head and pumping capacity. In order to understand how the performance degradation process occurs, it is necessary to analyze the dynamics of the gas phase inside the rotor. Thus, the present work aims to study the behavior of isolated gas bubbles inside the rotor channels of a centrifugal pump. For this purpose an experimental setup was developed, which allows flow visualization inside the rotor channels. The test pump is constructed from a transparent material and a GoPro® camera attached to the rotor shaft was used to acquire images of the bubbles in a rotating reference frame. Additionally, the bubbles diameters and trajectories were obtained by employing an image processing and a tracking algorithm. Results shows that the bubble trajectory depends on the operational conditions, rotating speed and liquid flow rate.*

Keywords: *Centrifugal pumps, bubbles, flow visualization*

1. INTRODUCTION

Nowadays, one of the most widely used artificial lift techniques in the oil industry is the Electrical Submersible Pumps (ESPs). The ESP receives energy from an electric motor and transfers to the working fluid in the form of pressure. Due to the physicochemical characteristics of the oil wells, a high amount of gas can be pumped together with the oil.

For that, the presence of gas in the oil pumping is a problem that can lead to large losses of production due to the degradation in the performance of the pumps. Examples of performance curves of an ESP working in both single-phase and two-phase flow conditions (water and air) are shown in Fig. 1.

Several studies were carried out to verify the effects of different operational conditions such as intake gas volume fraction, intake pressure and interfacial tension between liquid and gas on the performance degradation of the ESPs (Gamboa, 2008; Lea and Bearden, 1982; Murakami and Minemura, 1974; Neuman et al., 2016; Poullikkas, 2003). These studies have shown that increasing gas volume fraction in an ESP yields the formation of large gas pockets inside the pump rotor channels. This condition leads to an abrupt drop of the pump performance, which is generally associated to surging. However, most of the studies were performed in closed rotors without visual access, making difficult to analyze the gas phase dynamics. Although, most studies aimed to quantify the performance reduction due to the presence of gas into the pump, the bubbles dynamics due to the flow conditions into the rotor still now are poorly explored.

Murakami and Minemura, 1974, performed a force balance on a bubble into a rotor, where the authors suggested a balance between the drag force and the pressure gradient. Although the dynamics of gas bubbles in centrifugal pumps have already been observed (Murakami and Minemura, 1977; Murakami and Minemura, 1980; Stel et al., 2019), a better understanding of the forces acting on the gas bubbles and their response in the liquid phase inside a centrifugal pump it is still required.

Thus, this study presents a work on the analysis of single bubble motion, in which different bubble sizes were evaluated at different pump operating conditions. It is expected that, the findings shown in this work contribute on a better understanding on the behavior of the gas phase in a centrifugal pump.

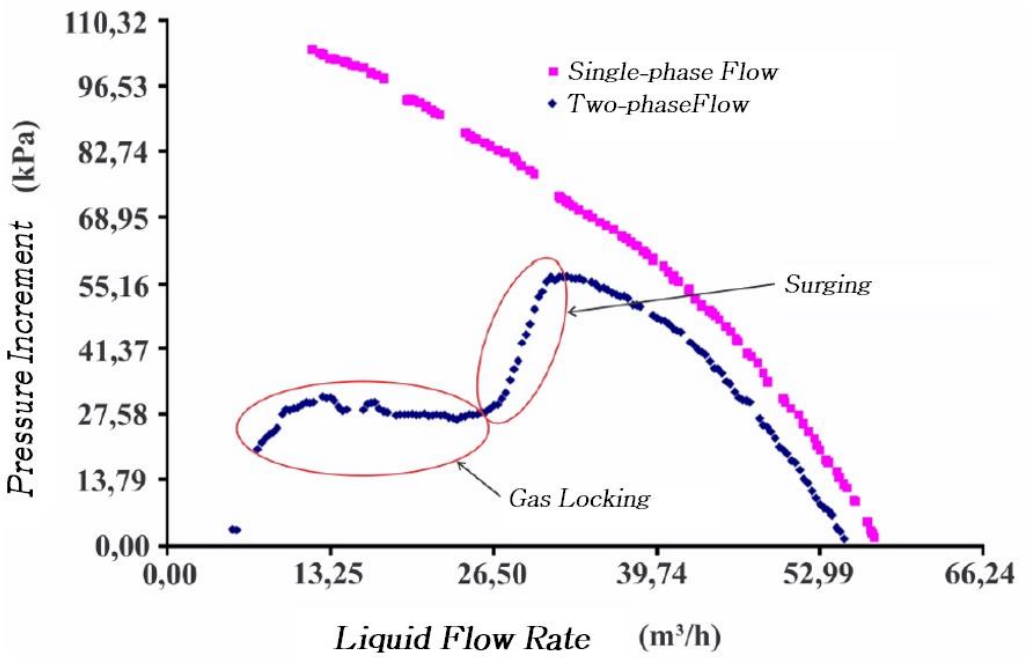

Figure 1. Typical performance curves of an ESP operating with two phase and single-phase flow (Cubas, 2017).

2. EXPERIMENTAL SETUP

In order to study an isolated bubble dynamics inside the rotor of an ESP, an experimental apparatus developed in the NUEM-UTFPR facilities was used (Fig. 2).

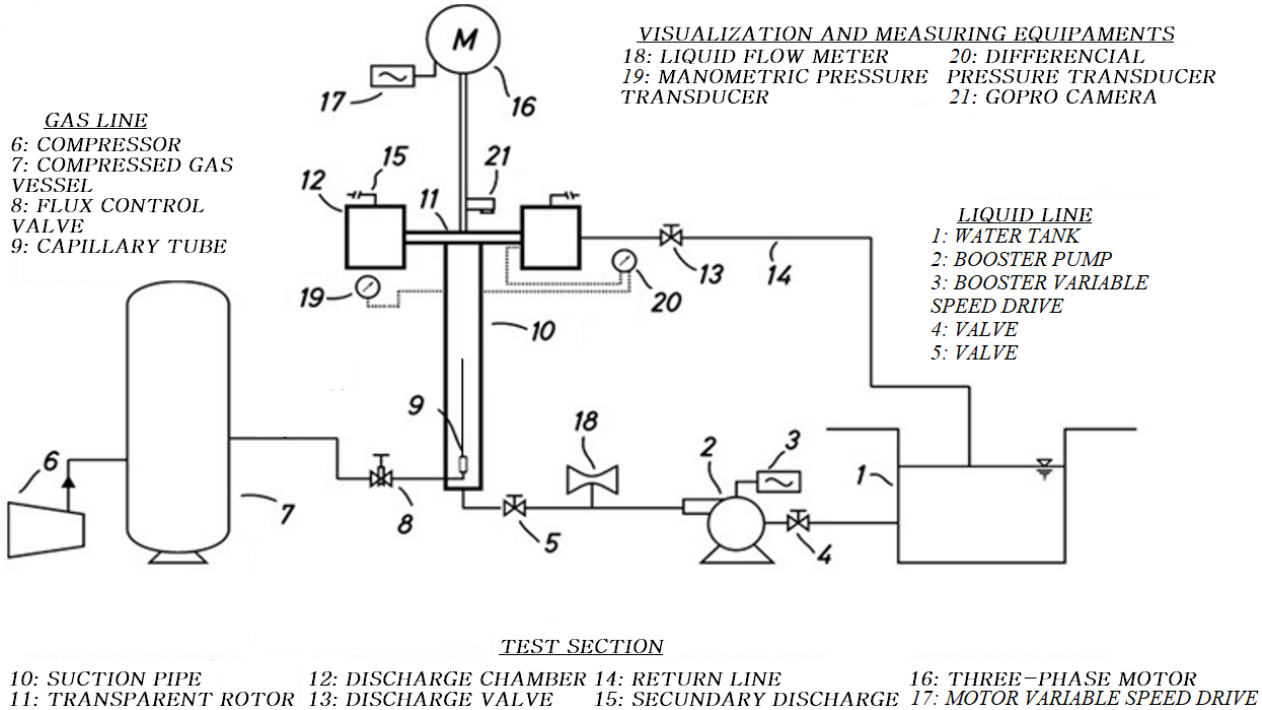

Figure 2. Experimental setup.

A booster pump (2) was employed to pump water to the test section through a liquid line. After the system is filled with water, compressed air is supplied by a compressor (6) through a vessel (7) to the test section.

In order to produce isolated bubbles, the air was injected by capillary tubes (9). The bubbles are generated at the beginning of the development pipe (10), which has internal diameter of $D_{in} = 70{,}1$ mm, and flow upwards along the liquid phase.

The flow is admitted axially into the rotor (11) and is discharged radially in a chamber (12). The flow is directed back to the tank via a return line (14), where the gas and the liquid phase are naturally separated by gravity. In order to remove some of the water and air from the system, a secondary outlet (15), located at the top of the discharge chamber, is also used to keep the outlet submerged in water.

The rotor is rotated through a shaft, which is connected to a three-phase motor (16), in which the speed is controlled by a variable speed drive (17). A Coriolis flow meter (18) is used to measure the liquid mass flow rate.

The intake pressure is measured by a gauge pressure transducer (20), located 1.77 D_{in} upstream of the rotor inlet, while the pressure rise of the rotor is measured by a differential pressure transducer (21), in which the outlet pressure port is at 10.8 mm downstream of the rotor outlet radius.

Images of the flow inside the rotor channel were taken by a camera (GoPro ®) (22), which is installed in the shaft of the pump. A set of LED lamps, positioned in the back of the rotor, is used to illuminate the rotor channels and enhance the contrast of the bubbles contour in the images.

In order to carry out the tests, the liquid flow rate and the pressure at the inlet of the rotor are regulated through the speed of the booster pump, using a variable speed drive (3), and by the opening or closing of a set of valves located in the return line (13,14). The gas flow rate is regulated with a needle valve (8).

The signals provided by flow rate meters and the pressure transducers are acquired through the Foundation Fieldbus® protocol, which are controlled and recorded using the LabView® software.

The camera is triggered through a wi-fi connection and the images are stored on an SD card inside the camera itself.

The gas was injected through capillary tubes with different internal diameters, which allows generating isolated bubbles of varied sizes.

The development pipe has a length between the capillary and the rotor of 17 D_{in}. A dynamic seal system is used to avoid leakage between the impeller and the fixed part (discharge chamber and development pipe).

The flow returns to the water tank through seven main lines and a secondary exit located at the top of the discharge chamber.

3. FLOW VISUALIZATION IN THE ROTOR CHANNELS

The experimental tests were carried out at a rotating speed of 200 rpm. Figure 3 presents a curve of flux coefficient, ψ, defined as $\psi = (\Delta P_{exp}/\rho_L)/(\omega D_{out})^2$ as a function of the load coefficient, ϕ, defined as $\phi = Q_L/(\omega D_{out}^3)$, where $D_{out} = 0{,}176$ m is the external diameter of the rotor and ΔP_{exp} is the static pressure gain measured experimentally. In addition, points (i), (ii), (iii) and (iv) correspond to the flow rates $0.5 \cdot Q_{BEP}$, $0.75 \cdot Q_{BEP}$, Q_{BEP} and $2 \cdot Q_{BEP}$, respectively, where the trajectories of the bubbles were evaluated. Three capillary tubes with different internal diameters were used for obtaining bubbles with three different diameters (approximately 1mm, 2mm and 3mm).

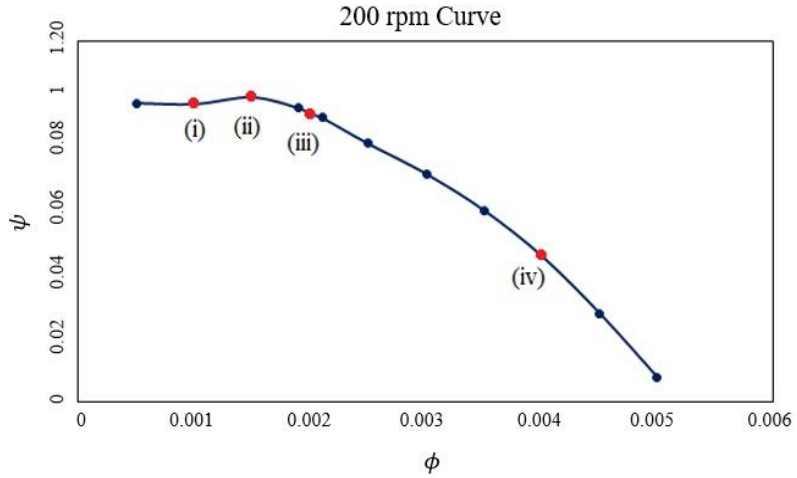

Figure 3. Curve of flux coefficient at 200 rpm as function of the load coefficient.

Figure 4 presents images of the bubble path in the impeller channel at 2· Q_{BEP} liquid flow rate and 200 rpm rotating speed for bubbles of approximately 1mm, 2mm and 3mm. At this liquid flow rate, the bubbles enters and leaves the impeller easily. It has been recognized that most significant forces acting on a single bubble in a centrifugal pump are the drag force and the pressure gradient force (Murakami and Minemura, 1974; Stel et al., 2019). At this point, the force due to the pressure gradient inside the channel is smaller than the drag force due to the velocity of the liquid phase, thus the bubble is dragged out of the impeller. However, the bubbles show oscillations in their trajectories, this could be due to the high turbulence of the liquid phase. In addition, at this point the bubbles with the largest diameters (3 mm) show a considerable deformation, a phenomenon that can also promotes oscillations in its trajectory and, in some cases, cause the breakup of the bubble.

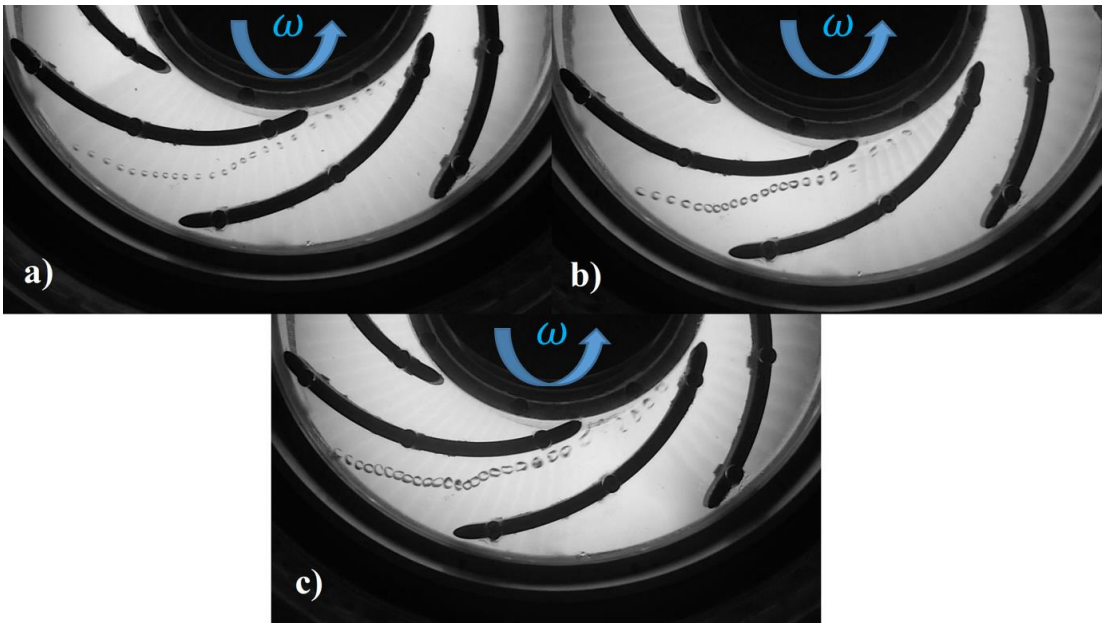

Figure 4. Images of the bubble path at 200 rpm rotating speed and 2·Q_{BEP} liquid flow rate for different bubble diameters 1 mm (a), 2 mm (b) and 3 mm (c).

In order to obtain the trajectories of the bubbles in the rotor channel, the videos acquired by the camera are separated in images frames, and these images are processed by a subroutine developed in MATLAB® software. This subroutine transforms the images in a gray scale to increase its contrast. Then, an image without the presence of bubbles is subtracted from a set of images in which bubbles are flowing through the channel. The resulting images are binarized, in this manner the algorithm is able to recognize the closed contour of the bubbles. This process performed successively frame by frame, thus obtaining the trajectory of a bubble.

Figure 5 shows the bubbles trajectory taken from the image processing at the same condition of Fig. 4. The bubbles have a similar trajectory, despite the increase in the bubble diameter. It was observed that the different bubbles enter to the rotor at approximately at the same position (almost in the middle of the blades). Then, they pass near the blade leading edge, and are deflected to the middle of the channel, exiting the impeller.

Figure 6 shows images of the bubbles paths at Q_{BEP} flow rate and a rotating speed of 200 rpm. In this case, the trajectories of the bubbles are quite different from Fig. 4. The bubbles seems to follow the liquid streamline of higher velocity, which is near the blade suction side. Close to the blade trailing edge, the bubble is deflected toward the blade pressure side and exit the impeller. However, for the bubble of 2 mm in diameter, the bubble touch the blade and then, it is dragged to the impeller outlet. For this liquid flow rate, the turbulence is expected to be lower and only small deformations are observed in comparison to the 2·Q_{BEP} case. The drag force is still dominant over the pressure gradient force and all bubbles are pushed to the impeller outlet.

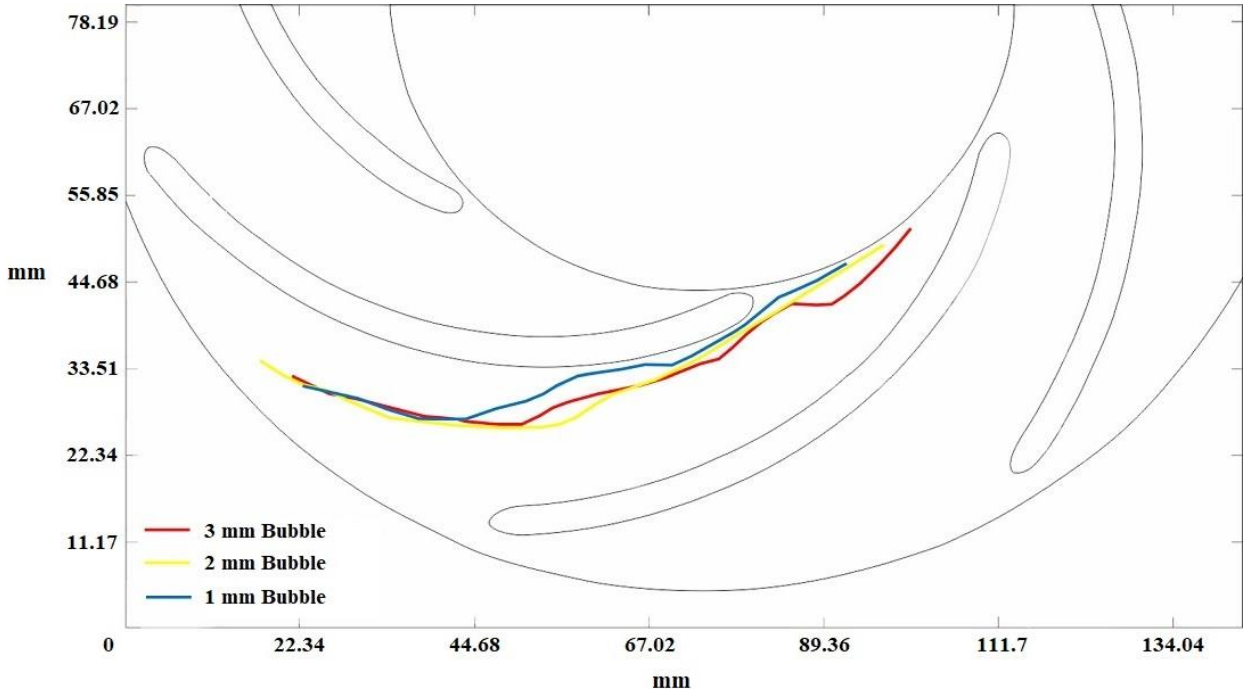

Figure 5. Bubble trajectories at $2 \cdot Q_{BEP}$ liquid flow rate.

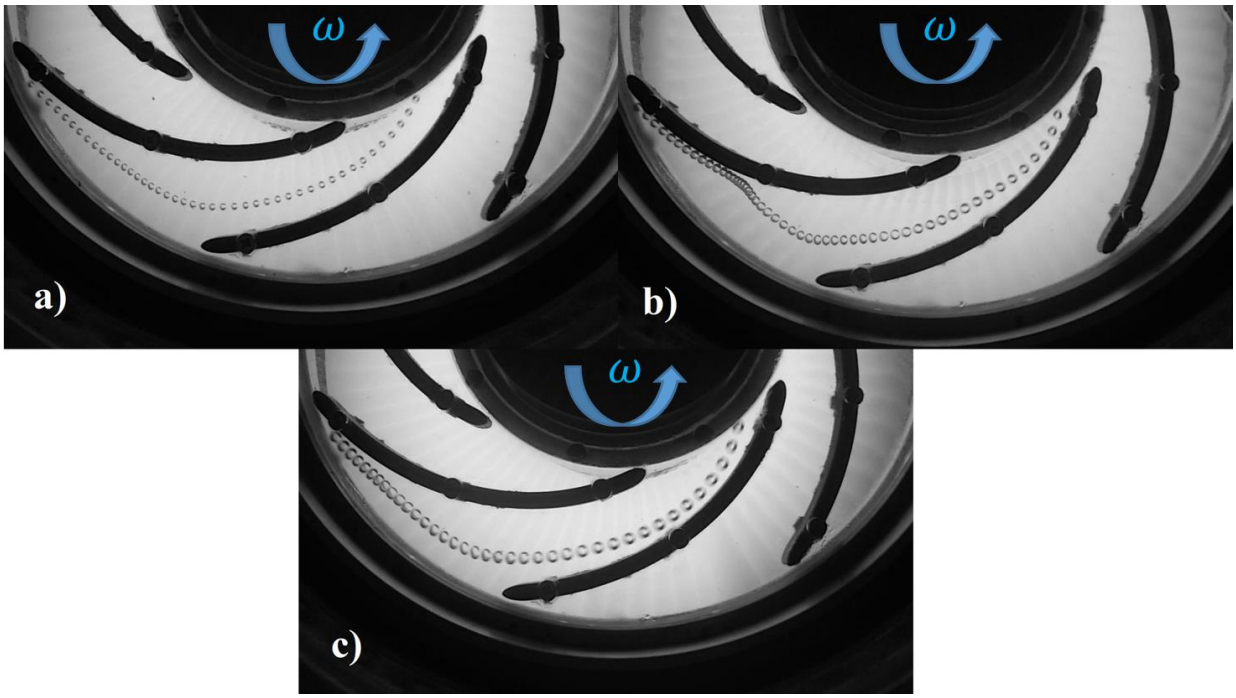

Figure 6. Images of the bubble path at 200 rpm rotating speed and Q_{BEP} liquid flow rate for different bubble diameters: 1 mm (a), 2 mm (b) and 3 mm (c).

Figure 7 shows the bubble trajectory obtained from the image processing at Q_{BEP} liquid flow rate. It can be noted that the bubbles have a similar trajectory despite the initial position, but small differences can be observed. The bubbles of 2 and 3 mm in size have almost the same initial position, but the 3mm bubble moves nearer the blade suction side than the 2mm bubble. In addition, the deflection suffered by the 2mm bubble is stronger than in the 1 and 3 mm bubbles, in which the bubble seemed to be attached to the blade pressure side.

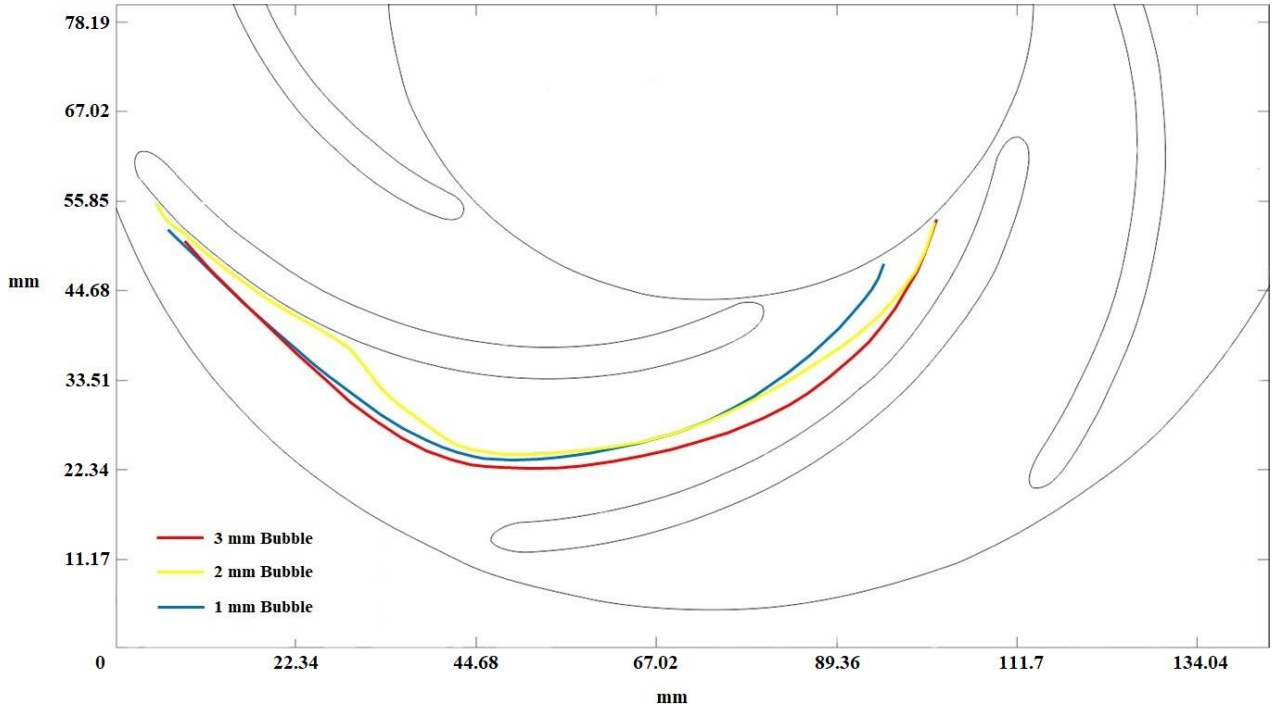

Figure 7. Bubble trajectories at Q_{BEP} liquid flow rate after performing the image processing.

Figure 8 shows images of the bubble trajectories at 200 rpm rotating speed and $0.75 \cdot Q_{BEP}$ liquid flow rate. In this case, all bubbles flows near the blade pressure side. The drag force is diminished and the pressure inside the impeller increases. This effect decelerates the bubble inside the impeller and it is pushed toward the pressure surface, in which it pushes the bubble toward the outlet. For this liquid flow rate, the turbulence around the bubble is small and its deformation is negligible.

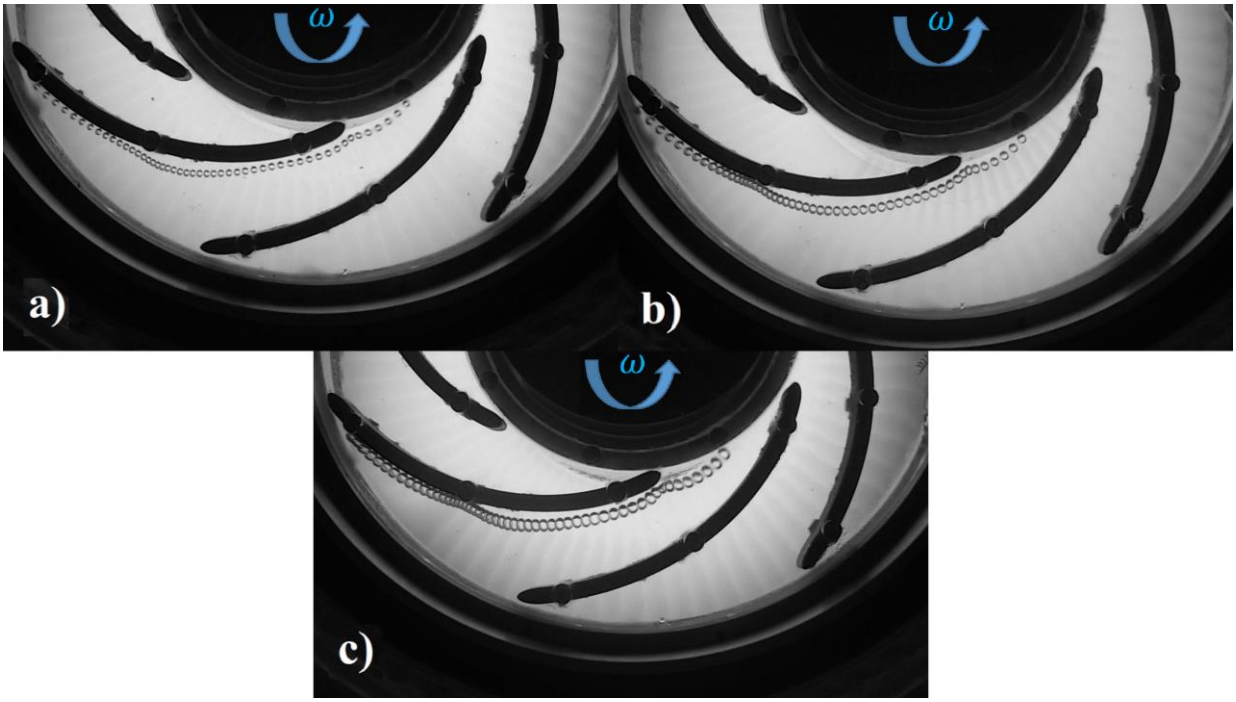

Figure 8. Images of the bubbles paths at 200 rpm rotating speed and $0.75 \cdot Q_{BEP}$ liquid flow rate for different bubble diameters: 1 mm (a), 2 mm (b) and 3 mm (c).

Figure 9 presents the bubble trajectories at $0.75 \cdot Q_{BEP}$ liquid flow rate generated by the image processing. The trajectories observed in Fig. 8 are similar for the three different bubble sizes. However, in this case, the bubbles are not deflect to the middle of the channel and flow very close to the blade pressure side. The initial position of the bubbles are almost the same and there is no significant differences in their trajectories, which means that, in this case, the bubble diameter has not influence over the trajectory. In addition, the bubbles are able to leave the impeller.

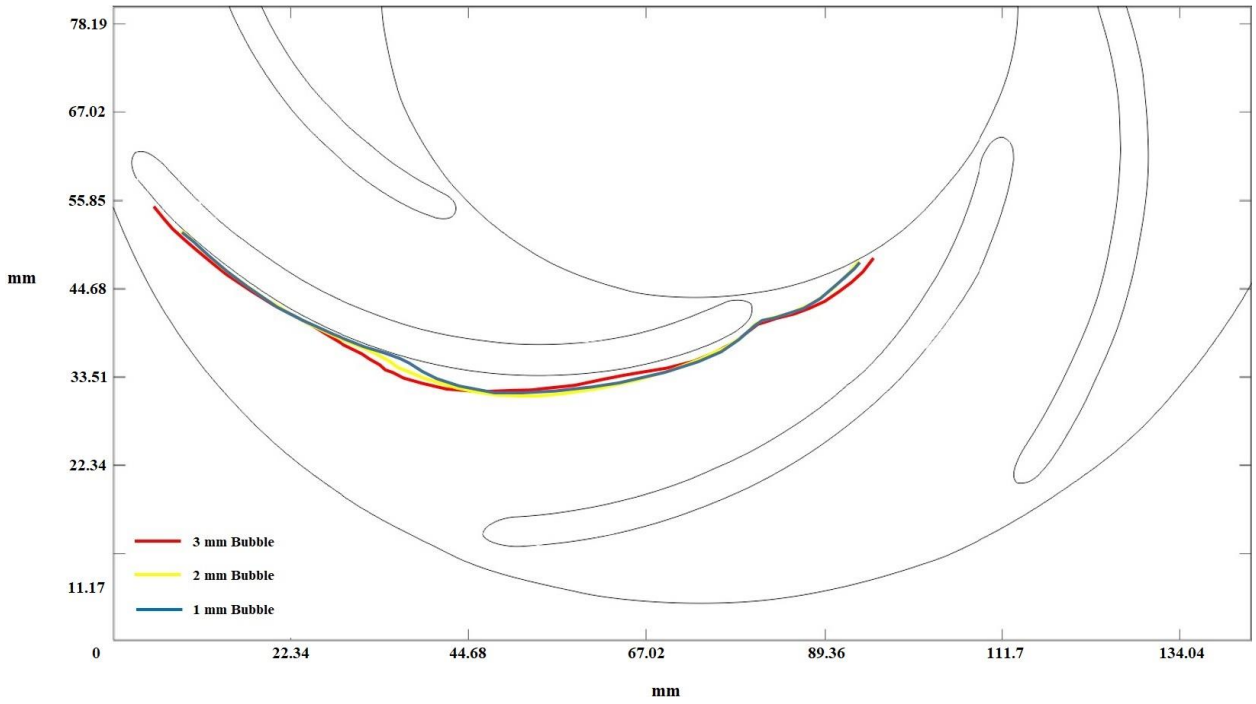

Figure 9. Bubble trajectories at $0.75 \cdot Q_{BEP}$ liquid flow rate after performing the image processing.

Figure 10 shows an image of bubble coalescence in the impeller channel. In this case, the bubbles are not able to leave the impeller immediately, as observed in the figures above. This can be due to the pressure gradient force that eventually surpass the drag force and the bubbles may be stagnated in the blade pressure side or move toward the inlet section. Then, other bubble that enters the rotor may shock with the stagnated bubble and coalesces. Eventually, some bubbles can leave the impeller.

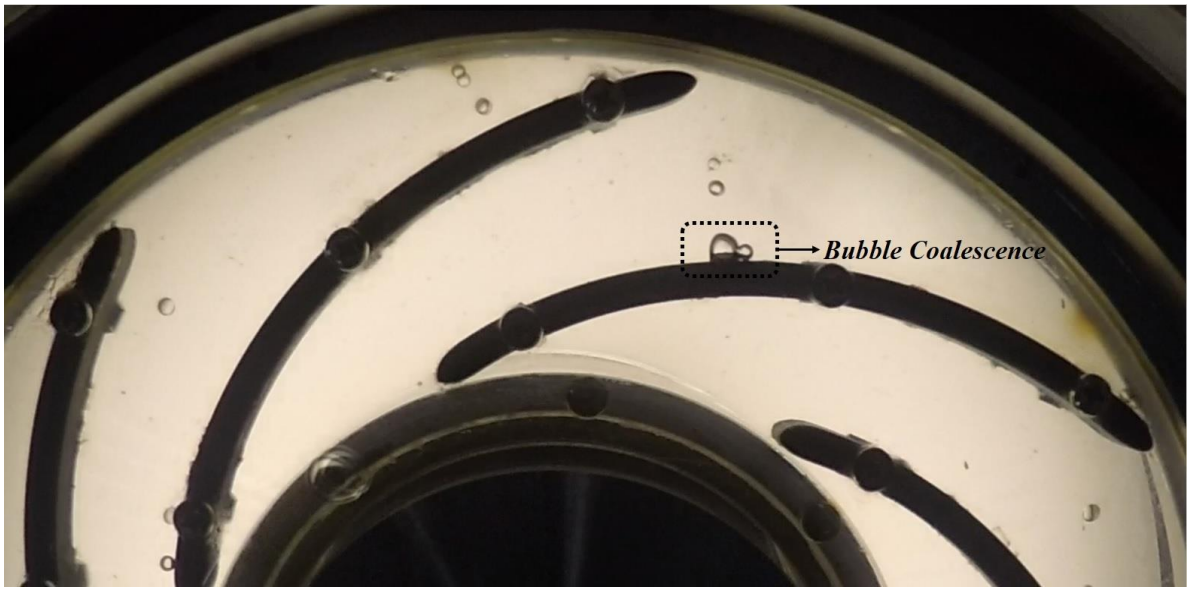

Figure 10. Image of bubble coalescence in the channel for $0.5 \cdot Q_{BEP}$ liquid flow rate point and 200 rpm rotating speed.

4. CONCLUSIONS

For a better understanding of the behavior of the gas phase inside the rotor of a centrifugal pump, an experimental study was carried out in which an analysis of isolated gas bubbles trajectories into the rotor channels was performed. Experimental tests were carried out for four different flow rates at 200 rpm rotating speed. Three capillaries tubes of different internal diameters were used as gas injectors, in order to generate bubbles of varied diameters. Bubbles of approximately 1 mm, 2 mm and 3 mm in diameter were obtained. From the results it can be inferred that the drag and pressure gradient forces lead the bubbles behavior. The former is dominant in flow rates above the BEP, while the latter dominates in liquid flow rate bellow BEP. Different trajectories were observed, but for the same liquid flow rate, the trajectories were found to be similar. Additionally, it was noted that, for the lowest liquid flow rate, bubble coalescence occurs, which indicates that the pressure gradient force has surpass the drag force. The present analysis is an effort to contribute to the understanding of the complex phenomena encounter in ESPs under two-phase flow conditions. However, more study have to be performed in order to investigate the influence of the rotating speed on the gas behavior inside such systems, which is an ongoing research.

5. REFERENCES

Cubas, J. M. C., 2017. “Estudo Experimental do Escoamento Bifásico Ar-Água em uma Bomba Centrífuga Radial”. Dissertação de Mestrado, UTFPR, Curitiba – Paraná, Brasil.

Gamboa, J., 2008. “Prediction of the Transition in Two-Phase Performance of an Electrical Submersible Pump”. Tese de Doutorado, The University of Tulsa, Oklahoma, EUA.

Lea, J. F.; Bearden, J. L., 1982. “Effects of Gaseous Fluids on Submersible Pump Performance”. *Journal of Petroleum Technology*, pp. 2922-2930.

Murakami, M.; Minemura, K., 1974. “Effects of Entrained Air on the Performance of a Centrifugal Pump”. *Bulletin of the JSME*, Vol. 17, No. 112, pp. 1047-1055.

Murakami, M.; Minemura, K., 1977. “Flow of Air Bubbles in Centrifugal Impellers and Its Effect on the Pump Performance”. *Proceedings of the 6th Australasian Hydraulics and Fluid Mechanics Conference*, Adelaide, Australia.

Murakami, M.; Minemura, K. A., 1980. “Theoretical Study on Air Bubble Motion in a Centrifugal Pump impeller”. asme journal of fluids engineering, Vol. 102, pp. 446-453.

Neumann, M; Schäfer, T.; Bieberle, A.; Hampel, U.,2016. “An Experimental Study on the Gas Entrainment in Horizontally and Vertically Installed Centrifugal Pumps”. *Journal of Fluids Engineering*, Vol. 138, pp. 091301.

Poullikkas, A., 2003. “Effects of Two-Phase Liquid-Gas Flow on the Performance of Nuclear Reactor Cooling Pumps”. *Progress in Nuclear Energy*, Vol. 42, pp. 3-10.

Stel, H.; Ofuchi, E. M.; Sabino, R. H. G.; Ancajima, F. C.; Bertoldi, D.; Marcelino, M. A.; Morales, R. E. M., 2019. “Investigation of the Motion of Bubbles in a Centrifugal Pump Impeller”. *ASME Journal of Fluids Engineering*, doi:10.1115/1.4041230.

6. RESPONSIBILITY NOTICE

The authors are the only responsible for the printed material included in this paper.